Wu *et al.*
Chinese Journal of Mechanical Engineering (2023) 36:54
https://doi.org/10.1186/s10033-023-00871-z

Chinese Journal of Mechanical Engineering

ORIGINAL ARTICLE

Open Access

Numerical Simulation Investigation on Parameter Optimization of Deep-Sea Mining Vehicles

Hongyun Wu[1], Wei Liu[1], Min Jiang[1,2], Changfeng Li[3], Jiangming Li[1], Bingzheng Chen[1], Chunlai Wang[3*] and Yuheng Chen[1]

Abstract

The four-track walking mining vehicle can better cope with the complex terrain of cobalt-rich crusts on the seabed. To explore the influence of different parameters on the obstacle-crossing ability of mining vehicles, this paper took a certain type of mine vehicle as an example and establish a mechanical model of the mine vehicle. Through this model, the vehicle's traction coefficient variation could be analyzed during the obstacle-crossing process. It also reflected the relationship between the obstacle-crossing ability and the required traction coefficient. Many parameters were used for this analysis including the radius of the guide wheel radius, ground clearance of the driving wheel, the dip angle of the approaching angular and the position of centroid. The result showed that the ability to cross the obstacles requires adhesion coefficient as support. When the ratio between obstacle height and ground clearance of the guide wheel was greater than 0.7, the required adhesion coefficient increased sharply. The ability to cross obstacles will decrease, if the radius of the guide wheel increases, the height of the driving wheel increases or the dip angle of the approaching angular increases. It was most beneficial to cross the obstacle when the ratio of the distance between the center of mass and the front driving wheel to the wheelbase is between 0.45–0.48. The results of this paper could provide reference for structural parameter design and performance research for mining vehicles.

Keywords Rich crusts, Four-track vehicles, Triangular track, Obstacle-crossing

1 Introduction

Cobalt rich crust is a kind of deep sea solid mineral resource with great value which is rich in Mn, C, Pt and other metal elements [1, 2]. It is mainly distributed on the flat top and steep slopes of seamounts and seamounts in the Pacific Ocean with a depth of 1000–3500 m [3]. According to incomplete statistics, potential resources of the cobalt rich crust deposits in the western Pacific volcanic belt are one billion tons, the amount of cobalt metal is several million tons, and the total economic value has exceeded 100 billion US dollars [4–6]. Since the 1980s, the cobalt rich crust has been a hotspot in the research and development of the world's marine mineral resources, but the terrain of cobalt rich crust mining area is complex, which is not conducive to the walking of mining vehicles [7, 8]. Relevant scholars at home and abroad had formed a representative towing, self-propelled, winch traction, articulated crawler, planetary wheel, composite wheel for the mining vehicle [9, 10]. Some design schemes have completed the walking test, but the field test has not been carried out [11]. The four-track mining vehicle used four triangular track as walking device. Each

*Correspondence:
Chunlai Wang
clwang@cumtb.edu.cn
[1] Institute of Marine Research, Changsha Mining Research Institute Co., Ltd., Changsha 410012, China
[2] School of Mechanical and Electrical Engineering, Central South University, Changsha 410083, China
[3] School of Energy and Engineering, China University of Mining & Technology Beijing, Beijing 100083, China

crawler wheel was driven separately and all the track could swing around the driving wheel, so it could better adapt to the complex topography of the cobalt rich crust mining area. It has a strong ability to cross obstacles and may be used for mining cobalt-rich crusts [12, 13].

At present, there are many researches on the obstacle-crossing performance of tracked vehicles at home and abroad [14]. Xu et al. [15] studied the propulsion resistance of crawler mining vehicles based on the coupled rheological model and obtained a new calculation formula for the traction force of crawler mining vehicles. The track spacing and the contact length on the steering traction were analyzed. Xu used RecurDyn software and self-programming subroutine to calculate the shear-shear rheological sinking of crawler-type mining vehicles at different speeds, and realized the compression-shear combined rheological constitutive model. Li et al. [16] established a single track shoe with grouser driving model to optimize the track structural parameters and improved the tractive performance of the tracked mining vehicle on soft sediments. Feng et al. [17] proposed a planetary wheeled walking mode, which used the transformation of fixed axle trains and planetary gear trains to improve the ability to cross the obstacles. The author established the obstacle-crossing motion of planetary-wheel-type walking mechanism based on the principle of virtual work, and analyzed the influence of the structure size of planetary gear train, the position of vehicle body center and adhesion coefficient on the height of obstacle-crossing. The change of the load on the track was complicated and there was a big impact in the process of obstacle-crossing. Li et al. [18] studied and analyzed the obstacle-crossing mechanism of the sea-bottom swing-arm crawler obstacle-crossing vehicle, also the three dimensional dynamic model of the vehicle was established by using ADAMS/ATV software and the process of obstacle-crossing was simulated. Chen et al. [19] analyzed the obstacle-crossing performance of the displacement four-track-foot robot, and established the constraint condition and solved the maximum obstacle height under the specified parameters. Zhu et al. [20] established a thermo-hydro-mechanical dynamic response model of saturated porous deep-sea sediments under vibration of mining vehicles, based on Green-Lindsay (G-L) generalized thermoelasticity theory and Darcy's law. Xu et al. [21] established a compression-shear coupled rheological constitutive model of sediment simulants using internal time theory, and deduced a new formula for calculating the steering traction force of tracked mining vehicles. The effects of slewing speed, track spacing and length of track and deep-sea sediment contact on slewing traction are analyzed.

However, the adhesion coefficient provided by the ground was assumed to be sufficient in the model, but it was practical that the adhesion coefficient of cobalt rich crusts was limited. So that it cannot be applied to the conditions of crusts. In this paper, the obstacle-crossing performance of four-track mining vehicle was studied in stages. By analysis each of the obstacle-crossing stage, the relationship between the height of obstacle-crossing and the required traction coefficient was obtained. Intuitively judge the change in difficulty level in the process of obstacle-crossing. On this basis, the influence of the parameters such as the approaching angular of the track wheel, ground clearance of the driving wheel, the radius of the guide wheel and the position of the centroid on the obstacle-crossing performance was analyzed under a certain design parameter. It could provide theoretical support for the research and design of obstacle-crossing performance of four-track mining vehicle.

2 Model of Four-Track Mining Vehicle for Cobalt-rich Crust

The schematic view of the structure of a four-track mining vehicle is shown in Figure 1. The main body was composed of a frame, four triangular track, a hydraulic station and four traveling motor. Each of the triangular track is rigidly connected to the frame by a hydraulic motor, and each of the triangular track can swing around the driving wheel by a certain angle. To prevent the turning, the swing angle is restrained by the limiting device. When the left and right motors were at the same speed, the mining vehicle went straight; when the left and right motors at different speeds, the mining vehicle turned.

The triangular track was a widely used in recent years. Rubber is used as the track material, so the weight is light and the grounding specific pressure is small. At the same time, the periodic fluctuation of the tension of the traditional steel track is avoided, so the efficiency is higher. A common structure of the triangular track is shown in

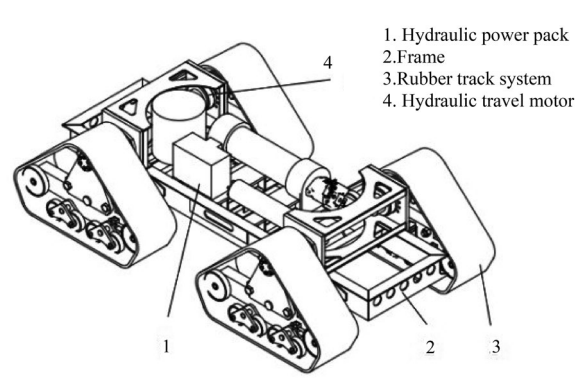

Figure 1 The structure of four-tracked mining vehicle

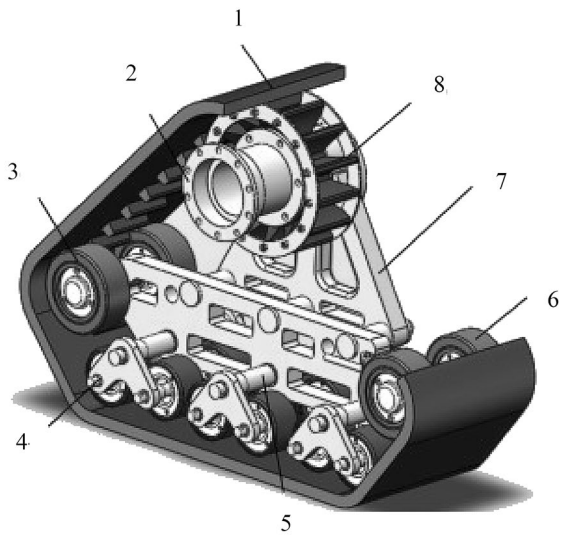

1. Rubber track 2.Connecting flange 3. Idler 4.Track roller 5.Compensating beam 6. Tensioning wheel 7.Truck frame 8.Driving wheel

Figure 2 Structure of triangular track

Figure 2. The guide wheel and the thrust wheel are similar to the conventional track. But the driving wheels are placed higher to ensure sufficient ground clearance and improve pass ability. The triangular track is driven by meshing the driving wheel with the shoe teeth on the inner side of the rubber track [22–30]. In the process of obstacle crossing, the triangular crawler not only moves horizontally with the vehicle and rotates around the front and rear axles, but also swings around the driving wheel, and the swing angle needs to be limited to prevent overturning, which makes the obstacle crossing process more complex [31].

3 Obstacle-Crossing Analysis of Four-Track Mining Vehicle

The topographical features of the cobalt rich crust can be simplified into a combination of flat, slope and step. Among them, the step-crossing can best reflect the obstacle-crossing performance of mining vehicles [30–32]. Figure 3 shows the Obstacle-crossing process of four-track mining vehicle in seabed cobalt rich crust mining area. As the four-track mining vehicle moves, the guiding wheel began to contact the step and the frictional force caused the track to generate a turning moment. The guide wheel is lifted, and then the approaching angular

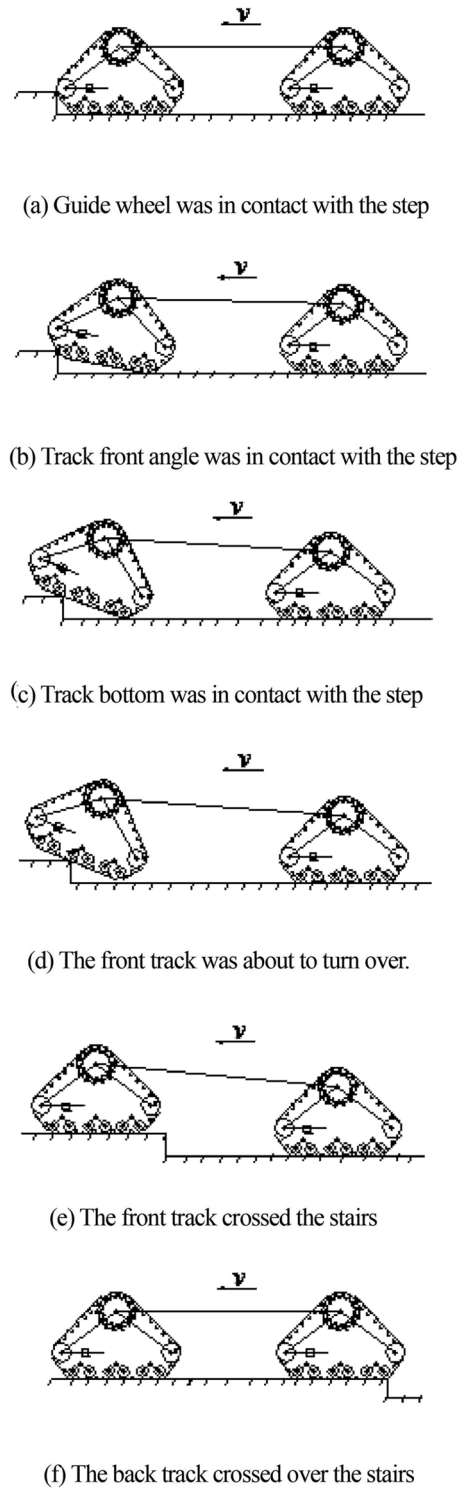

Figure 3 Schematic diagram of obstacle-crossing for four-track vehicle

began to contact with the step, and then the crawler track is in contact with the step. As the four-track mining vehicle walk forward, the whole front track passes over the step [13], and then the rear track repeats the above process. It must be completed in each stage to ensure that the four-track mining vehicle can successfully cross the obstacle. Because the stress state of each stage is different, it needs to be modeled and solved separately.

For the needs of research, the whole step process was simplified as follows:

1. The terrain of cobalt rich crust is hard ground, and the ground conditions are consistent;
2. The rubber crawler does not stretch during the stepping process;
3. The motor has sufficient driving force;
4. Since the mining vehicle traveling speed is usually less than 0.8 m/s, the rigid impact is not considered in this model.
5. The four-track mining vehicle has enough ground clearance and does not interfere with the steps.

3.1 Obstacle-Crossing Condition of the Vehicle

When the vehicle over the obstacle, the horizontal component of the restraint reaction force of the obstacle to the mining vehicle was balanced with the horizontal component of the traction force. The traction coefficient is introduced as φ [21], let $\varphi = F/N$, where F is the total traction force and N is the total ground reaction force in the formula. It is assuming that the adhesion coefficient provided by friction between the cobalt rich crust terrain and crawler surface as $\varphi_{\max_{\max}}$, then the obstacle-crossing condition is $\varphi \le \varphi_{\max}$. That is, the traction coefficient at any stage cannot exceed the adhesion coefficient, otherwise the obstacle crossing will fail.

3.2 Mechanical Model of Four-Track Vehicle in Obstacle-Crossing Process

3.2.1 Mechanical Model of the Front Track when the Guide Wheel Contacts the Step

As shown in Figure 4, it is the force analysis model of the obstacle-crossing process when the guide wheel contacts the step. Assuming that the step height is h_w, the dip angle of approaching angular of the triangular track is β, the ground clearance of the guide wheel is h_s, the ground clearance of the driving is h_z, the grounding length of the triangular track is m, the positive pressure of the contact position of the guide wheel and the step is F_{11}, the positive pressure at the position where the front track is in contact with the ground is F_{12} and the positive pressure at the rear track is F_2, The F_2 is usually in surface contact. It is generally considered to be evenly distributed, so F_2 could be simplified as a concentrated force, which located in the geometric center of the grounding section of the track. η is defined as the difference value between the traction coefficient φ and the rolling resistance coefficient f, that is $\eta = \varphi - f$, G is the gravity of the four-track mining vehicle, a is the distance between the center of mass and the front driving wheel, b is the distance between the center of mass and the rear driving wheel, L is the wheelbase.

At the beginning of the guide wheel contact the step, the angle between the the track and the ground very small. It is still assumed that the front crawler remains in contact with the ground completely. The mining vehicle is balanced in the horizontal and vertical directions. The force balance equation, the moment balance equation and the front track torque balance equation of the overall horizontal and vertical directions of the four-track are respectively established, and the supplementary equations are established according to the geometric relations as follows:

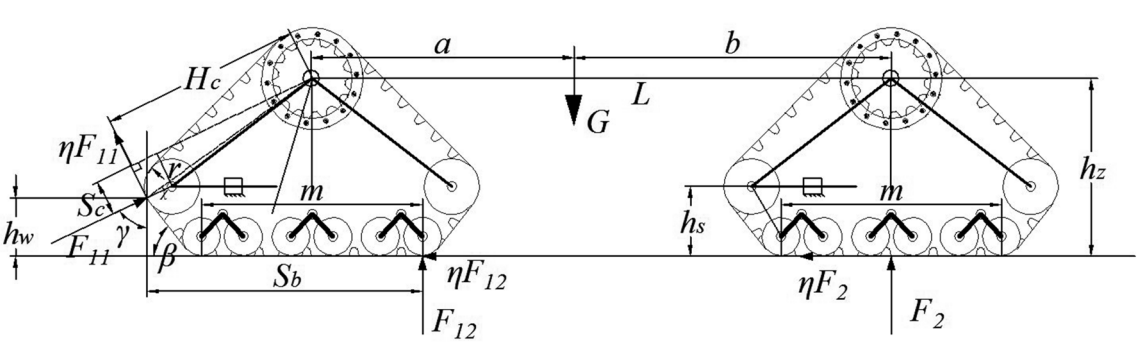

Figure 4 Mechanical model of the front track when the guide wheel contacts the step

$$
\begin{cases}
F_{11}(\eta\sin\gamma+\cos\gamma)+F_2+F_{12}=G,\\
\eta F_{11}\cos\gamma+\eta F_2+\eta F_{12}=F_{11}\sin\gamma,\\
\eta F_2 h_w+\eta F_{12}h_w+G(a+S_b-m/2)=F_2\left(L+S_b-\dfrac{m}{2}\right)+F_{12}S_b,\\
\eta F_{11}H_c+\eta F_{12}h_z=F_{11}S_c+F_{12}m/2,\\
S_b=\dfrac{h_w}{\tan\beta}+m,\\
\cos\chi=\dfrac{(h_z-h_w)^2-(h_z-h_s)^2+\left(\frac{m}{2}+\frac{h_w}{\tan\beta}\right)^2-\left(\frac{m}{2}+\frac{h_s}{\tan\beta}\right)^2+2r\left(\frac{m}{2}+\frac{h_s}{\tan\beta}\right)}{2r\sqrt{\left(\frac{m}{2}+\frac{h_w}{\tan\beta}\right)^2+(h_z-h_w)^2}},\\
S_c=\sqrt{\left(\dfrac{m}{2}+\dfrac{h_w}{\tan\beta}\right)^2+(h_z-h_w)^2}\sin\chi,\\
H_c=\sqrt{\left(\dfrac{m}{2}+\dfrac{h_w}{\tan\beta}\right)^2+(h_z-h_w)^2}\cos\chi,\\
\cos\gamma=\dfrac{h_s-h_w}{r},\\
\eta=\varphi-f.
\end{cases}
\tag{1}
$$

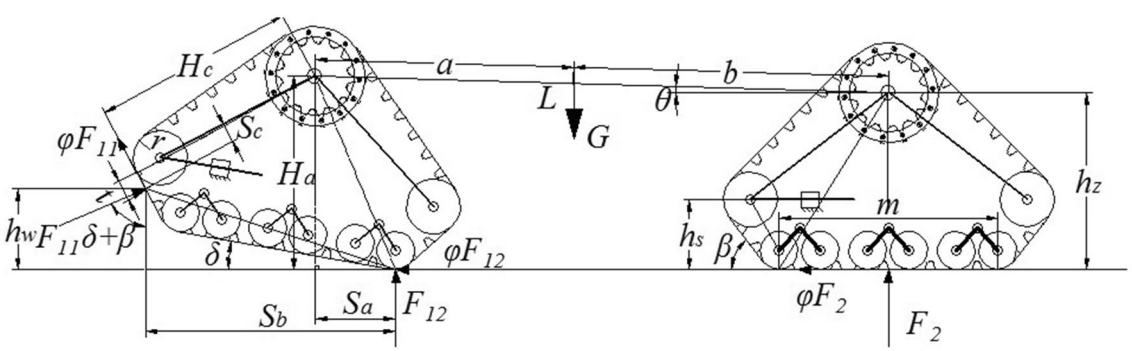

Figure 5 Mechanical model of the front track when the approaching angular contacts the step

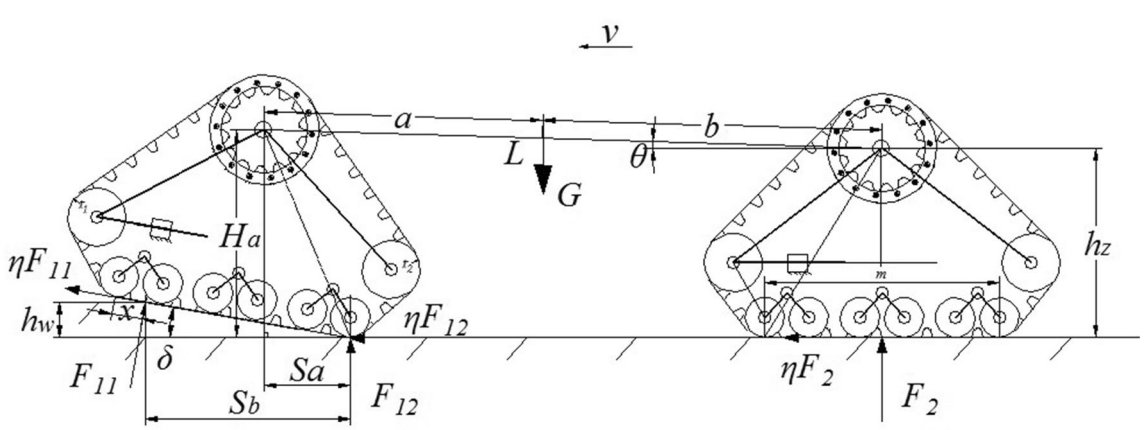

Figure 6 Mechanical model of the front track when the bottom of the crawler contacts the step

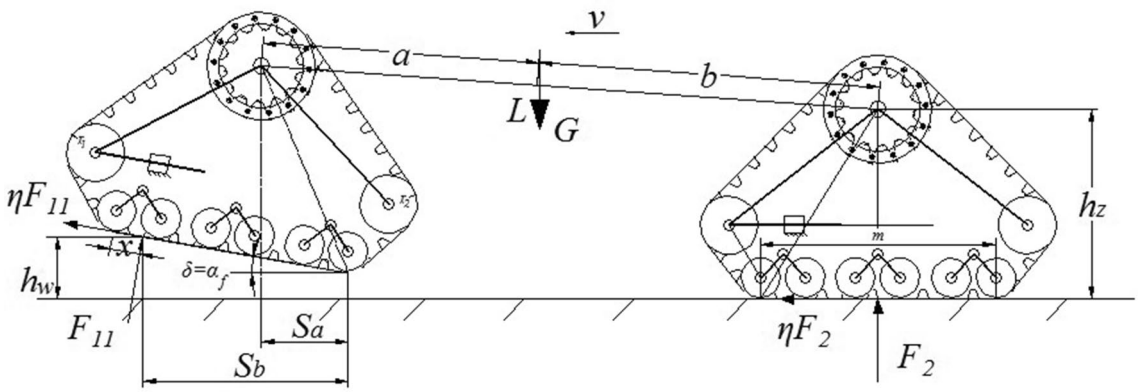

Figure 7 The static model of the obstacle-crossing when the front track swing exceeds limit angle

In Eq. (1), the unknown included the traction coefficient φ, F_{11}, F_{12}, F_2. The known quantity includes the track's geometric and the step height h_w, The r represents the angle between F_{11} and the vertical direction. Using Eq. (1), we can find that when r was from β to π/2, the values of φ, F_{11}, F_{12} and F_2.

3.2.2 Mechanical Model of the Front Track when the Approaching Angular Contacts the Step

As shown in Figure 5, it is the force analysis model of the approaching angular of the front track in the process of contact the step. It is assumed that the angle of the track lift is δ, the angle of the body lift is θ and the other parameters are consistent with the previous definitions.

In the process of approaching angular contacting the step, the balance equations, the moment balance equation and the front track torque balance equation of the overall four-track mining vehicle are established respectively, the supplementary equation is established according to the relationship as follows:

$$\begin{cases} \eta F_{11}\sin(\delta+\beta)+F_{11}\cos(\delta+\beta)+F_2+F_{12}=G, \\ \eta F_{11}\cos(\delta+\beta)+\eta(F_2+F_{12})=F_{11}\sin(\delta+\beta), \\ (\eta F_{12}+\eta F_2)h_w+G(a\cos\theta+S_b-S_a)=F_2(L\cos\theta+S_b-S_a)+F_{12}S_b, \\ \eta F_{11}H_c+\eta F_{12}H_a=F_{11}S_c+F_{12}S_a, \\ c=\sqrt{\left(\dfrac{h_s-r\cos\beta}{\sin\beta}-t\right)^2+m^2+2m\left(\dfrac{h_s-r\cos\beta}{\sin\beta}-t\right)\cos\beta}, \\ \delta=\arcsin\dfrac{h_w}{c}-\arcsin\dfrac{h_s-r\cos\beta}{c}, \\ S_c=\sqrt{\left(\dfrac{m}{2}\right)^2+h_z^2}\cos\left(\pi-\beta-\arctan\dfrac{2h_z}{m}\right)-\dfrac{h_s-r\cos\beta}{\sin\beta}+t, \\ H_c=\sqrt{\left(\dfrac{m}{2}\right)^2+h_z^2}\sin\left(\pi-\beta-\arctan\dfrac{2h_z}{m}\right), \\ S_a=\sqrt{\left(\dfrac{m}{2}\right)^2+h_z^2}\cos\left(\delta+\arctan\left(\dfrac{2h_z}{m}\right)\right), \\ H_a=\sqrt{\left(\dfrac{m}{2}\right)^2+h_z^2}\sin\left(\delta+\arctan\left(\dfrac{2h_z}{m}\right)\right), \\ S_b=\sqrt{c^2-h_w^2}, \\ \sin\theta=\dfrac{H_a-h_z}{L}. \end{cases} \tag{2}$$

In Eq. (2), the unknown includes the traction coefficient φ, F_{11}, F_{12}, F_2. The known quantity includes the track's geometric and the step height h_w. t represents the linear distance from the starting point of the approaching angular to the contacting point of the step. The values of the unknown number such as φ, F_{11}, F_{12}, and F_2 could be calculated by Eq. (2) when the value of t was taken from 0 to $h_s - r\cos\beta/\sin\beta$.

3.2.3 Mechanical Model of the Front Track when the Bottom of the Crawler Contacts the Step

As shown in Figure 6, it is the force analysis model when the bottom of the crawler of the front track in the process of contacting the step.

In this process, the balance equations of the overall horizontal and vertical directions of the four-track, the moment balance equation and the front track torque balance equation are established respectively and the supplementary equations are established according to the geometric relationship as follows:

$$\begin{cases} F_{11}(\eta\sin\delta+\cos\delta)+F_2+F_{12}=G, \\ \eta F_{11}\cos\delta+\eta F_2+\eta F_{12}=F_{11}\sin\delta, \\ \eta F_2 h_w+\eta F_{12}h_w+G(S_b-S_a+a\cos\theta) \\ \quad =F_2(S_b-S_a+L\cos\theta)+F_{12}S_b, \\ F_{11}(m/2-x)+\eta F_{11}h_z+\eta F_{12}H_a=F_{12}S_a, \\ \delta=\arcsin\left(\dfrac{h_w}{m-x}\right), \\ S_b=\dfrac{h_w}{\tan\delta}, \\ S_a=\sqrt{\left(\dfrac{m}{2}\right)^2+h_z^2}\cos\left(\delta+\arctan\left(\dfrac{2h_z}{m}\right)\right), \\ H_a=\sqrt{\left(\dfrac{m}{2}\right)^2+h_z^2}\sin\left(\delta+\arctan\left(\dfrac{2h_z}{m}\right)\right), \\ \sin\theta=\dfrac{H_a-h_z}{L}. \end{cases} \tag{3}$$

In Eq. (3), the unknown includes the traction coefficient φ, F_{11}, F_{12}, F_2. The known quantity includes the track's geometric and the step height h_w. x represents the linear distance from the starting point of the crawler surface to the contacting point of the step. The values of the unknown number such as φ, F_{11}, F_{12}, and F_2 could be calculated by Eq. (3) when x was taken from 0 to m. When the calculated value of F_{12} was less than or equal to 0, it means that the track is flipped before the occurrence of the track and the obstacles-crossing is successfully.

3.2.4 Static Model of the Obstacle-Crossing when the Front Track Swing Exceeds Limit Angle

In the model established in the above stage, it assumes that the swing angle of the triangular truck around the driving wheel did not exceed the limit angle. As shown in Figure 7, when the track was turned forward to reach the angle of the rollover and the F_{12} is still calculated to be greater than 0 according to Eq. (3), while the track is not turned over. But the limit device made the second half of the track will leave the ground. The situation is abrupt and must be modeled separately.

In the process of the front track grounding step after reaching the specified angle, the balance equation, the torque balance equation of the overall horizontal and vertical directions of the four-track are respectively established. The supplementary equation is established according to the geometric relationship as follows:

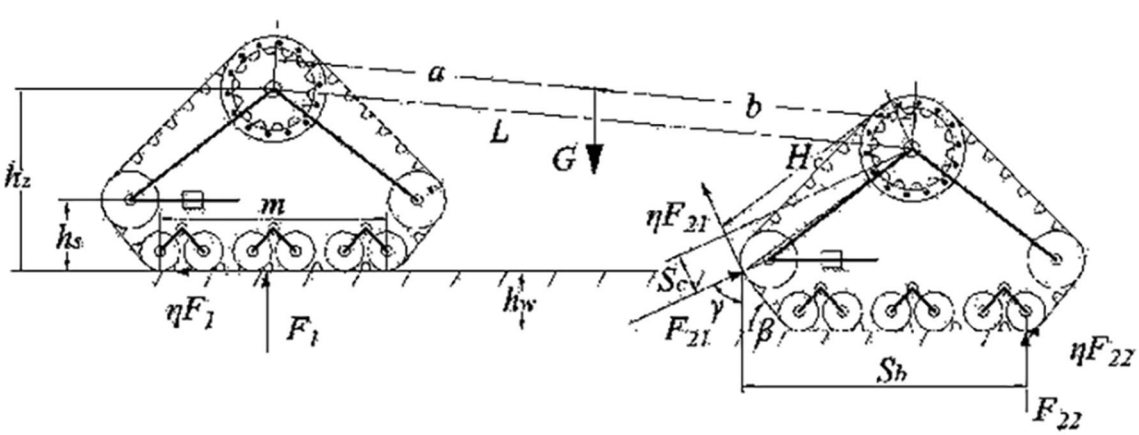

Figure 8 Force analysis model of the obstacle-crossing process when the guide wheel of the rear track contacts the step

$$\begin{cases} F_{11}(\eta \sin\alpha_f + \cos\alpha_f) + F_2 = G, \\ \eta F_{11}\cos\alpha_f + \eta F_2 = F_{11}\sin\alpha_f, \\ \eta F_2 h_w + G(S_b - S_a + a\cos\theta) = F_2(S_b - S_a + L\cos\theta), \\ S_b = (m - x)\cos\alpha_f, \\ S_a = \sqrt{\left(\frac{m}{2}\right)^2 + h_z^2}\cos\left(\alpha_f + \arctan\left(\frac{2h_z}{m}\right)\right), \\ H_a = \sqrt{\left(\frac{m}{2}\right)^2 + h_z^2}\sin\left(\alpha_f + \arctan\left(\frac{2h_z}{m}\right)\right) + h_w - (m - x)\sin\alpha_f, \\ \sin\theta = \frac{H_a - h_z}{L}, \\ \eta = \varphi - f. \end{cases} \tag{4}$$

In Eq. (4), the unknown included the traction coefficient φ, F_{11}, F_2. The known quantity includes the track's geometric and the step height h_w. x represents the linear distance from the starting point of the crawler surface to the contacting point of the step. The value of the unknown numbers φ, F_{11}, and F_2 when the value of x changes from 0 to m can be obtained by Eq. (4). When the calculated value of F_{11} and the resultant force direction of ηF_{11} pass through the center of the driving wheel, it indicates that the step ends.

Eqs. (1)–(4) established the calculation formula of the traction coefficient φ and the ground support force under the condition that the step height is known during the obstacle-crossing process of the vehicle.

3.2.5 Mechanical Model of the Rear Track in Obstacle-Crossing Process

The obstacle-crossing process of the rear track is similar to that of the front track. The guide wheel of the rear track contacts the step first, then the approaching angular of the rear track contacts the step, and then the bottom of the crawler contacts the step. Finally, the whole four-track vehicle completes the obstacle-crossing process. After the front track crosses the steps, the connecting part will turn a certain angle, which will change the stress state of the four-track vehicle during obstacle-crossing. Since the obstacle crossing process of the rear track is similar to that of the front track, only the process of the guide wheel crossing the steps is analyzed, and other models will not be repeated.

As shown in Figure 8, it is the force analysis model of the obstacle-crossing process when the guide wheel of the rear track contacts the step. Assuming that the step height is h_w, the dip angle of approaching angle of the triangular track is β, the angle of the front track lift is θ', the ground clearance of the guide wheel is h_s, the ground clearance of the driving is h_z, the grounding length of the triangular track is m, the positive pressure of the contact position of the guide wheel and the step is F_{21}, the positive pressure at the position where the rear track is in contact with the ground is F_{22} and the positive pressure

Table 1 Parameters of the four-track mining vehicle

Parameter name	Value
Vehicle weight G (N)	38000
Drive wheelbase distance H_z (mm)	716
Front and back track wheelbase L (mm)	1900
Guide wheelbase ground distance h_s (mm)	326
Distance between center of gravity and front axle a (mm)	900
Driving resistance coefficient f	0.18
Guide wheel radius r (mm)	180
Triangular track guide wheel approach angle β (°)	38
Caterpillar length m (mm)	866
Track overturn limitation α_f (°)	15

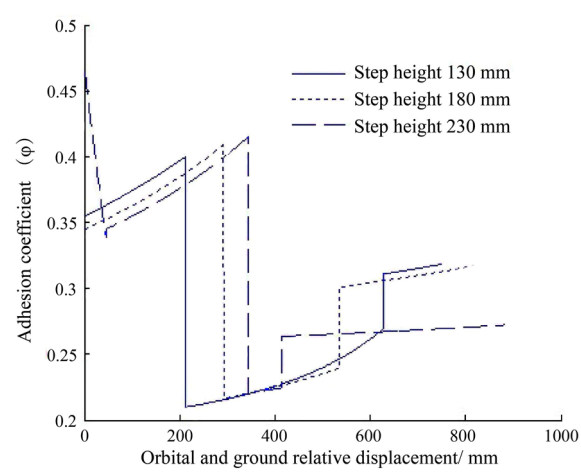

Figure 9 Variation of traction coefficient of front track during obstacle-crossing

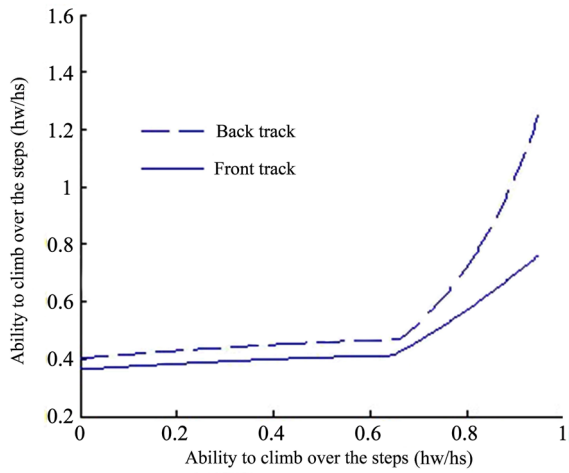

Figure 10 The correspondence relationship between obstacle-crossing ability and traction coefficient

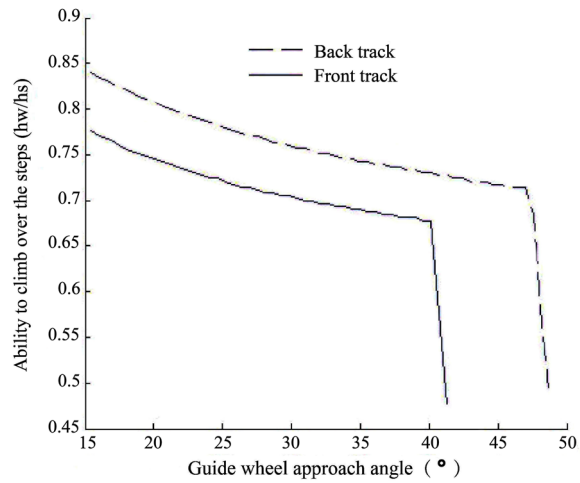

Figure 12 Influence of guide wheel diameter on obstacle-crossing ability

at the front track is F_1. The F_1 is usually in surface contact. It is generally considered to be evenly distributed, so F_1 could be simplified as a concentrated force, which located in the geometric center of the grounding section of the front track. η is defined as the difference value between the traction coefficient φ and the rolling resistance coefficient f, that is $\eta=\varphi-f$, G is the gravity of the four-track mining vehicle, a is the distance between the center of mass and the front driving wheel, b is the distance between the center of mass and the rear driving wheel, L is the wheelbase.

The force balance equation, the moment balance equation and the rear track torque balance equation of the overall horizontal and vertical directions of the four-track are respectively established, and the supplementary equations are established according to the geometric relations as follows:

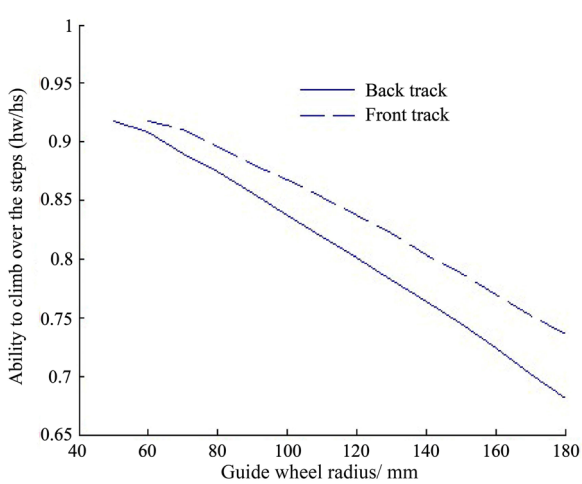

Figure 11 Influence of guide wheel diameter on obstacle-crossing ability

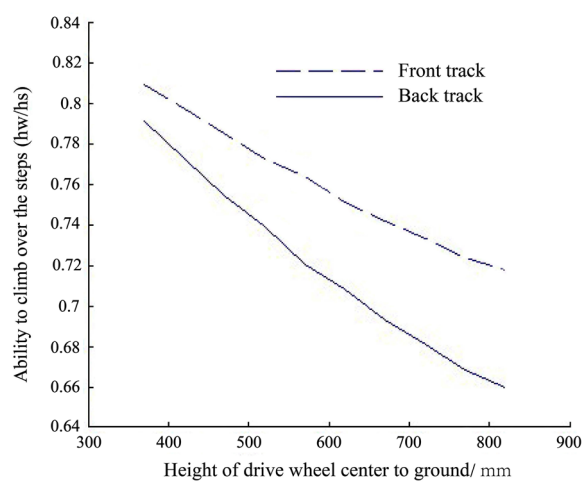

Figure13 Influence of the ground clearance of the driving wheel on obstacle-crossing ability

$$\begin{cases} F_{21}(\eta\sin\gamma+\cos\gamma)+F_1+F_{22}=G, \\ \eta F_{21}\cos\gamma+\eta F_1+\eta F_{22}=F_{21}\sin\gamma, \\ \eta F_{22}h_w+F_1\left(L\cos\theta'-S_b+\dfrac{m}{2}\right)=F_{22}S_b+G(b\cos\theta'+S_b-m/2), \\ \eta F_{21}H_c+\eta F_{22}h_z=F_{21}S_c+F_{22}m/2, \\ S_b=\dfrac{h_w}{\tan\beta}+m, \\ \cos\chi=\dfrac{(h_z-h_w)^2-(h_z-h_s)^2+\left(\frac{m}{2}+\frac{h_w}{\tan\beta}\right)^2-\left(\frac{m}{2}+\frac{h_s}{\tan\beta}\right)^2+2r\left(\frac{m}{2}+\frac{h_s}{\tan\beta}\right)}{2r\sqrt{\left(\frac{m}{2}+\frac{h_w}{\tan\beta}\right)^2+(h_z-h_w)^2}}, \\ S_c=\sqrt{\left(\dfrac{m}{2}+\dfrac{h_w}{\tan\beta}\right)^2+(h_z-h_w)^2}\sin\chi, \\ H_c=\sqrt{\left(\dfrac{m}{2}+\dfrac{h_w}{\tan\beta}\right)^2+(h_z-h_w)^2}\cos\chi, \\ \cos\gamma=\dfrac{H_s-h_w}{r}, \\ \eta=\varphi-f, \end{cases} \tag{5}$$

In Eq. (5), the unknown included the traction coefficient φ, F_{21}, F_{22}, F_1. The known quantity includes the track's geometric and the step height h_w, The r represents the angle between F_{21} and the vertical direction. Using Eq. (5), we can find that when r was from β to π/2, the values of φ, F_{21}, F_{22} and F_1.

3.3 Solution and Analysis of Obstacle-Crossing Process of Four-Track Vehicle

Taking a certain type of four-track vehicle as a model, the change of traction coefficient during the whole obstacle-crossing process and the relationship between obstacle-crossing ability and traction coefficient were solved by numerical simulation software. The basic structural parameters of four crawler mining vehicle are shown in Table 1.

3.3.1 Variation of Traction Coefficient of Front Track during Obstacle-Crossing

The step height h_w was assumed to be 130 mm, 180 mm and 230 mm respectively. The variation process of traction coefficient was solved and analyzed. The results are shown in Figure 9. When the height of the step was 230 mm, traction coefficient curve was composed of four parts, which corresponded to the step (a), (b), (c) and (d) four parts. When the step height was 130 mm and 180 mm, the traction coefficient curve consisted of three parts, corresponding to the step (a), (b), (c) three stages. This was because when the step height was 130 mm and 180 mm, the guide wheel edge of the track was higher than the step. When the step height was 230 mm, the guide wheel of the track could contact the step. From the curve trajectory, when the step height was 230 mm, the traction coefficient required to contact the step was the largest, which reached 0.46. As the step progresses, the required traction coefficient first decreased and then increased, when it was just touching the step, it was the smallest, then increased slowly. When it reaches the flip angle, the required traction coefficient suddenly increased, and then slowly increased until the end of the step. When the height was 130 and 180 mm, and the end of the approach angle was in contact with the step, the required adhesion coefficient was the largest, which were 0.40 and 0.42 respectively. When the bottom of the crawler contacts the step, the traction coefficient was the minimum.

Through the above analysis, it can be analyzed the three positions where the crawler may fail during obstacle crossing:

1. When the guide wheel just contact the step;
2. When the end position of the approaching angular contact the step;
3. When the bottom of the crawler was about to cross the step.

3.3.2 Relationship between Traction Coefficient and Obstacle-Crossing Ability of Front and Rear Tracks

The obstacle-crossing ability was defined as the ratio of the step height h_w to the height h_s of the center of the guide wheel from the ground. Gradually increase the step height from 0, and solve the corresponding traction coefficient under any step height according to the parameters in Table 1. The relationship between the obstacle-crossing ability and the traction coefficient φ was obtained as shown in Figure 10. When the ratio of step height to guide wheel height was less than 0.7, the required traction coefficient only increased slowly. This is because the guide wheel did not touch the step. When the ratio of the step height to guide wheel height exceeded 0.7, the required traction coefficient increases sharply.

It can also be analyzed from Figure 10 that when the mass center of the four-track vehicle is located at its geometric center, the traction coefficient required by the rear track is always greater than that of the front track, which means that the rear track is more difficult to cross obstacles.

4 Impact of Mining Vehicle Design Parameters on the Ability to Obstacles-Crossing

4.1 The Maximum Obstacle-Crossing Ability of the Mining Vehicle

The parameter of Table 1 was brought into the model in Section 3.3 to calculate the corresponding traction coefficient φ at different step height. The step height was gradually increased from 0. The maximum value of the traction coefficient φ was calculated under a certain step height. When $\varphi = \varphi_{\max}$, the step height at this time is the limit step height, and the ratio of the step height h_w to h_s the height of the center of gravity of the guide wheel was defined as the maximum obstacle ability at this time.

4.2 Influence of Design Parameters on Ability of Obstacle-Crossing

To measure the influence of the parameters, it was assumed that the adhesion coefficient of the cobalt-rich crust is 0.5, and the influence of some parameters on the maximum obstacle-crossing ability of the mining vehicle can be calculated by introducing Section 3.3.

4.2.1 Influence of the Radius of Guide Wheel on Ability of Obstacle-Crossing

The relationship between the maximum ability of step and the guide wheel radius was shown in Figure 11. The ability of the mining vehicle to step decreases with the radius of the guide wheel increased. So that the increase of the guide wheel was disadvantageous for the step. However, if the guide wheel was too small, it would cause the local radius of curvature of the track to increase and causing heat. Therefore, the actual engineering design should be selected as appropriate.

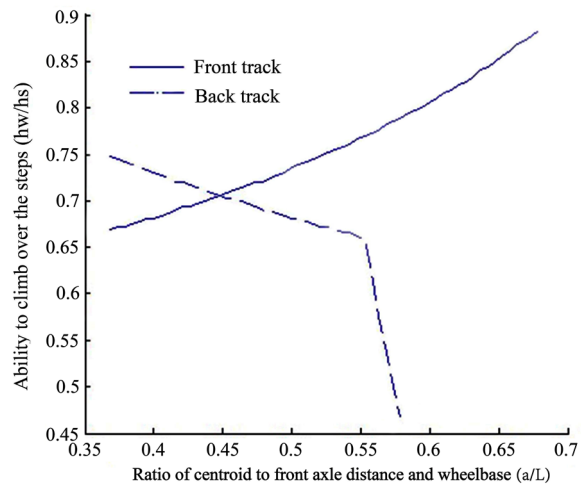

Figure 14 Influence of centroid position on ability of obstacle-crossing ability

4.2.2 Influence of the Dip Angle of Approach Angular on Ability of Obstacle-Crossing

The relationship between maximum ability to climb over the step and guide wheel approach angle was shown in Figure 12. As the approach angle increased the maximum ability to climb over the step decreases slowly. When the approach angle was greater than 40°, the maximum ability decreased sharply as the approach angular increased. Therefore, the approach angular should not exceed 40°.

4.2.3 Influence of the Ground Clearance of the Driving Wheel on Ability of Obstacle-Crossing

The relationship between the maximum ability to climb over the step and the ground clearance of the driving wheel was as shown in Figure 13. The ability of the mining vehicle to cross the step decreases as the height of the driving wheels increased from the ground. However, the driving wheel height off the ground too low will lead to a smaller clearance, which was not conducive to rough terrain walking. Therefore, in the actual design, the ground clearance should be appropriately increased.

4.2.4 Influence of Centroid Position on Ability of Obstacle-Crossing

The influence of centroid position on ability of obstacle-crossing ability was shown in Figure 14. When the

centroid moved backward, the ability of the front track to climb over the step increases. But under the same condition, the ability of the rear track decreases. Therefore, the position of the centroid should be as close as possible to the position of geometric center. when the ratio of the distance between the center of mass and the front driving wheel to the wheelbase is between 0.45–0.48, it was the most advantageous for obstacle-crossing.

5 Conclusions

(1) Established a mathematical model of the obstacle-crossing of the four-track mining vehicle, and obtained the traction coefficient variation curve required in the process of obstacle-crossing, so as to directly measure the change of difficulty in the process of obstacle crossing.
(2) When the ratio of step height to guide wheel height was less than 0.7, the traction coefficient increased slowly. When it exceeded 0.7, the traction coefficient increased sharply. The analysis also showed that when the center of gravity was in the geometric center, the obstacle-crossing difficulty of the rear track of the vehicle was greater than that of the front track.
(3) The influence of design parameters of four-track mining vehicle on obstacle-crossing ability was analyzed by model. The result shows that the ability of obstacle-crossing will decrease, when the radius of the guide wheel, the ground clearance of the driving wheel or the approaching angular increased. When the centroid position moved forward, it was unfavorable for the obstacle-crossing of the front track, but it was more favorable for rear track, and vice versa. When the ratio of the centroid distance from the front axle to the wheelbase that was between 0.45 and 0.48, it was the most advantageous for obstacle- crossing. The above conclusions provided a reference for the design of four-track mining vehicle.

Acknowledgements
Not applicable.

Authors' Contributions
HW and CW contributed to the design of the study, conducted the experiments, wrote and revised the manuscript. WL and MJ wrote the manuscript. CL and JL conducted the experiments and data analysis. BC and YC analyzed the data and figures. All authors read and approved the final manuscript.

Authors' Information
Hongyun Wu, born in 1976, is the Deputy Director of *Deep Sea Mining Technology Research Center, Changsha Institute of Mining Research Co. Ltd., China*. He received his PhD degree in 2010 from *Central South University, China*. His research focuses on exploration and mining technology and its equipment development of seabed mineral resources.
Wei Liu, born in 1988, is currently an engineer at *Changsha Institute of Mining Research Co. Ltd., China*. He received his master degree from *Changsha Institute of Mining Research Co. Ltd., China*, in 2018. His research interests include deep sea mining technology and equipment.
Min Jiang, born in 1987, is currently a PhD candidate at *Central South University, China*. He received his master degree from North University of China, in 2014. His main research interests include Deep-sea solid mineral resources development technology and equipment.
Changfeng Li, born in 1995, is currently an engineer at *School of Energy and Engineering, China University of Mining & Technology Beijing*. He received his master degree on mining engineer in *China University of Mining & Technology Beijing*, in 2021.
Jiangming Li, born in 1993, is currently an engineer at *Changsha Mining Research Institute Co. Ltd., China*. He received his master degree from *Changsha Institute of Mining Research, China*, in 2019. His main research interests include deep-sea mining equipment and control.
Bingzheng Chen, born in 1987, is currently a senior engineer at *Changsha Mining Research Institute Co. Ltd., China*. He received his master degree from *Changsha Institute of Mining Research, China*, in 2021. His main research interests include deep-sea mining technology and equipment.
Chunlai Wang, born in 1976, is currently the Deputy Director of *Department of Resource Engineering, China University of Mining and Technology, Beijing*. He received his PhD degree from *University of Science and Technology Beijing, China*, in 2011. His main research direction is early warning and control of rockburst.
Yuheng Chen, born in 1996, is currently an engineer at *Changsha Mining Research Institute Co., Ltd., China*. He received his master degree from *Changsha Institute of Mining Research, China*, in 2021. His main research interests include intelligent control of underwater robots.

Funding
Supported by National Ocean Key Special Funds in 12th Five-Year Plan of China (Grant No. DY125-11-T-01) and National Natural Science Foundation of China (Grant No. 52074294).

Declarations

Competing Interests
The authors declare no competing financial interests.

Received: 23 February 2021 Revised: 18 May 2022 Accepted: 7 March 2023
Published online: 19 April 2023

References
[1] J Ju, Y L Feng, H Li, et al. Recovery of valuable metals and NaCl from cobalt-rich crust and industrial waste salt via roasting coupling technology. *Journal of Sustainable Metallurgy*, 2021, 7(4): 1-14. https://doi.org/10.1007/S40831-021-00464-X.
[2] J Ju, Y L Feng, H Li. Separation of Cu, Co, Ni and Mn from acid leaching solution of ocean cobalt-rich crust using precipitation with Na2S and solvent extraction with N235. *Korean Journal of Chemical Engineering*, 2022: 1-11. https://doi.org/10.1007/S11814-021-0919-9.
[3] S J Liu, C Liu, Y Dai. Status and progress on researches and developments of deep ocean mining equipments. *Journal of Mechanical Engineering*, 2014, 50(2): 8-18. (in Chinese)
[4] J R Wakefield, K Myers. Social cost benefit analysis for deep sea minerals mining. *Marine Policy*, 2016, 95: 346-355. https://doi.org/10.1016/j.marpol.2016.06.018.
[5] X M Chen, H Y Wu, L H Ding. Present research situation of exploitation technology of cobalt-rich crusts. *Mining Research & Development*, 2008, 28(06): 1-3+19. https://doi.org/10.13827/j.cnki.kyyk.2008.06.001.
[6] J Teague, M J Allen, T B Scott. The potential of low-cost ROV for use in deep-sea mineral, ore prospecting and monitoring. *Ocean Engineering*, 2017, 147: 333–339. https://doi.org/10.1016/j.oceaneng.2017.10.046.

[7] Y G Liu, G W He, H Q Yao. Global distribution characteristics of seafloor cobalt-rich encrustation resources. *Mineral Deposits*, 2013, 32(6): 1275-1284. https://doi.org/10.16111/j.0258-7106.2013.06.017.

[8] J S Chung. Deep-ocean mining technology III: Developments. *ISOPE Ocean Mining (& Gas Hydrates) Symposium*, ISOPE Cupertino, California, USA, 2009.

[9] D X Leng, S Shao, Y C Xie, et al. A brief review of recent progress on deep sea mining vehicle. *Ocean Engineering*, 2021:108565. https://doi.org/10.1016/J.OCEANENG.2020.108565.

[10] Q H Rao, Z L Liu, F Xu, et al. Research progress on characteristics of deep-sea soft sediment and walking performance of mining vehicle. *The Chinese Journal of Nonferrous Metals*, 2021, 31(10): 2795-2816. https://doi.org/10.11817/j.ysxb.1004.0609.2021-42120.

[11] X Ju, J X Zhou, H B Niu. Exploration of cobalt crusts on the seabed. *China Mining Magazine*, 2020, 29(s1): 559-562. https://doi.org/10.12075/j.issn.1004-4051.2020.S1.003.

[12] W Liu, H Y Wu, M Jiang, et al. Research on the differential steering performance of self-propelled four-tracked vehicle using in seabed. *Mining Research and Development*, 2017, 37(11): 81-85. https://doi.org/10.13827/j.cnki.kyyk.2017.11.020.

[13] Y J Kang, S J Liu. The development history and latest progress of deep-sea polymetallic nodule mining technology. *Minerals*, 2021, 11(10): 1132-1132. https://doi.org/10.3390/MIN11101132.

[14] Q Su, H N Lv, J M Yang, et al. Analysis of the walking performance of tracked deep-sea mining vehicle on soft sediment. *Ocean Engineering*, 2022, 40(2): 162–168. https://doi.org/10.16483/j.issn.1005-9865.2022.02.016.

[15] F Xu, Q H Rao, W B Ma. Predicting the sinkage of a moving tracked mining vehicle using a new rheological formulation for soft deep-sea sediment. *Journal of Oceanology and Limnology (English)*, 2018, 36(2): 230-237. https://doi.org/10.1007/s00343-018-6344-1.

[16] J Li, S J Liu, Y Dai. Effect of grouser height on tractive performance of tracked mining vehicle. *Journal of the Brazilian Society of Mechanical Sciences and Engineering*, 2017, 39(7): 2459-2466. https://doi.org/10.1007/s40430-016-0641-4.

[17] Y L Feng, J Z Ma, W M Zhao. Obstacle performance of a plantary wheel mining vehicle in the deep sea bed. *Journal of University of Science and Technology Beijing*, 2009, 31(7): 923-928. https://doi.org/10.13374/j.issn1001-053x.2009.07.048.

[18] C Li, C Tuo, D Xiang. Obstacle surmounting performance of a swing-arm-type tracked seabed walking platform. *Journal of Central South University (Science and Technology)*, 2015, 46(7): 2481-2486.

[19] W Chen, L M Mao. Analysis of climbing obstacle capability of the parallel-robot with four tracked feet. *Machine Design & Research*, 2006, (06): 28-31. https://doi.org/10.13952/j.cnki.jofmdr.2006.06.008.

[20] W Zhu, X Y Shi, R Huang, et al. Research on coupled thermo-hydro-mechanical dynamic response characteristics of saturated porous deep-sea sediments under vibration of mining vehicle. *Applied Mathematics and Mechanics*, 2021, 42(9), 1349-1362. https://doi.org/10.1007/S10483-021-2768-5.

[21] F Xu, Q H Rao, W B Ma. Turning traction force of tracked mining vehicle based on rheological property of deep-sea sediment. *Transactions of Nonferrous Metals Society of China*, 2018, 28(6): 1233-1240. https://doi.org/10.1016/S1003-6326(18)64761-2.

[22] Z N Hu. Design on the rubber track wheel conversion. *IEEE International Conference on Computing*, 2011, https://doi.org/10.1109/CCIENG.2011.6008072.

[23] W Sanngeon, N Afzulpurkar, J Bhuripanyo, et al. Adaptive geometry track design and implementation for an all terrain mobile robot. *IEEE International Conference on Robotics & Biomimetics*, 2009, https://doi.org/10.4028/www.scientific.net/AMR.308-310.513.

[24] Hwa Kim. Development of a torque distribution algorithm for improving stability and mobility of the wall-climbing robot platform (ROPE RIDE) equipped with triangular track wheels. *Journal of the Korean Society for Precision Engineering*, 2013, 30: 725-732.

[25] J W Xing, H W Pu, X Z Meng, et al. Lightweight design for a new tracked triangular wheel structure. *Advanced Materials Research*, 2013, 744: 78-82. https://doi.org/10.4028/www.scientific.net/AMR.744.78.

[26] Z H Zhao, X H Mu, H L Guo. Test and modeling on static ground pressure of rubber track conversion system. *Transactions of the Chinese Society of Agricultural Engineering*, 2018, 34(3): 72-79

[27] Zhenning Hu. Optimization design in the driving gear wheel axle of triangular rubber track conversion. *Advanced Materials Research*, 2011, 308-310: 513-516.

[28] H L Guo, X H Mu, X Y Yang. Mechanics properties analysis and test of four rubber tracked assembly vehicle steering system. *Transactions of the Chinese Society of Agricultural Engineering*, 2016, 32(21): 79-86. https://doi.org/10.11975/j.issn.1002-6819.2016.21.011.

[29] Y W Li, S R Ge, H Zhu. Obstacle-surmounting mechanism and capability of four-track robot with two swing arms. *Robot*, 2010, 32(2): 157-165. https://doi.org/10.3724/SP.J.1218.2010.00157.

[30] J H Liu, W Gu, Z L Meng. Analyses and simulation study on obstacle surmounting and passing performance of submarine mining vehicle on slope. *Machinery*, 2018, 56(11): 56-59.

[31] B S Choi, S M Song. Fully automated obstacle-crossing gaits for walking machines. *IEEE Transactions on Systems, Man and Cybernetics*, 1988, 18(6): 952-964. https://doi.org/10.1109/21.23093.

[32] H Wu, X Chen, S Liu, et al. Influence of soft sediment adhered to track on adhesion performance of seabed track vehicle. *Transactions of the Chinese Society of Agricultural Engineering*, 2010, 26(10): 140-145. https://doi.org/10.3969/j.issn.1002-6819.2010.10.023.